ACSNANO

www.acsnano.org

ARTICLE

Engineered Diblock Polypeptides Improve DNA and Gold Solubility during Molecular Assembly

Nicole A. Estrich,*[,†] Armando Hernandez-Garcia,[‡,§] Renko de Vries,[§] and Thomas H. LaBean[†]

[†]Department of Materials Science and Engineering, North Carolina State University, Raleigh, North Carolina 27606, United States

[‡]Simpson Querrey Institute for Bionanotechnology, Northwestern University, Evanston, Illinois 60208, United States

[§]Laboratory of Physical Chemistry and Soft Matter, Wageningen University and Research Centre, Wageningen 6708 PB, The Netherlands

Supporting Information

ABSTRACT: **Programmed molecular recognition is being developed for the bionanofabrication of mixed organic/inorganic supramolecular assemblies for applications in electronics, photonics, and medicine. For example, DNA-based nanotechnology seeks to exploit the easily programmed complementary base-pairing of DNA to direct assembly of complex, designed nanostructures. Optimal solution conditions for bionanofabrication, mimicking those of biological systems, may involve high concentrations of biomacromolecules (proteins, nucleic acids, *etc.*) and significant concentrations of various ions (Mg^{2+}, Na^{+}, Cl^{-}, *etc.*). Given a desire to assemble diverse inorganic components (metallic nanoparticles, quantum dots, carbon nanostructures, *etc.*), it will be increasingly difficult to find solution conditions simultaneously compatible with all components. Frequently, the use of chemical surfactants is undesirable, leaving a need for the development of alternative strategies. Herein, we discuss the use of artificial, diblock polypeptides in the role of solution compatibilizing agents for molecular assembly. We describe the use of two distinct diblock polypeptides with affinity for DNA in the stabilization of DNA origami and DNA-functionalized gold nanoparticles (spheres and rods) in solution, protection of DNA from enzymatic degradation, as well as two 3D tetrahedral DNA origamis. We present initial data showing that the diblock polypeptides promote the formation in the solution of desired organic/inorganic assemblies.**

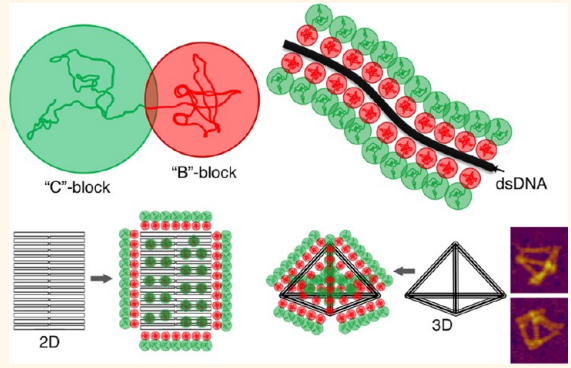

KEYWORDS: *directed self-assembly, molecular assembly, protein engineering, DNA nanotechnology, protein polymer, diblock polypeptide, solution compatibilization*

DNA-based nanotechnology utilizes properly designed molecular building blocks to reliably self-assemble into desired nanometer-scale constructs, bringing with them whatever chemical moieties and/or nanomaterials are covalently attached to them.[1,2] However, supramolecular assemblies containing building materials with diverse physicochemical properties must contend with very different interactions with solvent molecules and each other. Therefore, optimization of solution conditions to maximize solubility of one component may contradict the optimal conditions for other components and therefore create obstacles to high assembly yields.

In the case of DNA origami,[3−5] fairly high salt concentrations are commonly required (~12.5 mM Mg^{2+} or ~1.2 M NaCl)[6] to provide counterions for shielding of phosphate negative charges on the DNA backbone, allowing high charge densities to be tolerated within the tightly folded DNA origami structures. High salt concentrations are also commonly encountered in physiological samples (150 mM NaCl plus 260 mM KCl plus a few mM Mg^{2+}).[7−10] For gold nanoparticle (AuNP) systems, these high salt concentrations cause aggregation and precipitation due to the charge shielding that occurs, which reduces the electrostatic repulsion between neighboring AuNPs, allowing them to come in contact with one another, aggregate, and precipitate. In order to add more diverse components to these systems, such as carbon nanotubes, quantum dots, *etc.*, the problem of incompatible solution conditions will require a creative solution. For example, carbon nanotubes are

Received: October 28, 2016
Accepted: January 3, 2017
Published: January 3, 2017

DOI: 10.1021/acsnano.6b07291
ACS Nano 2017, 11, 831−842

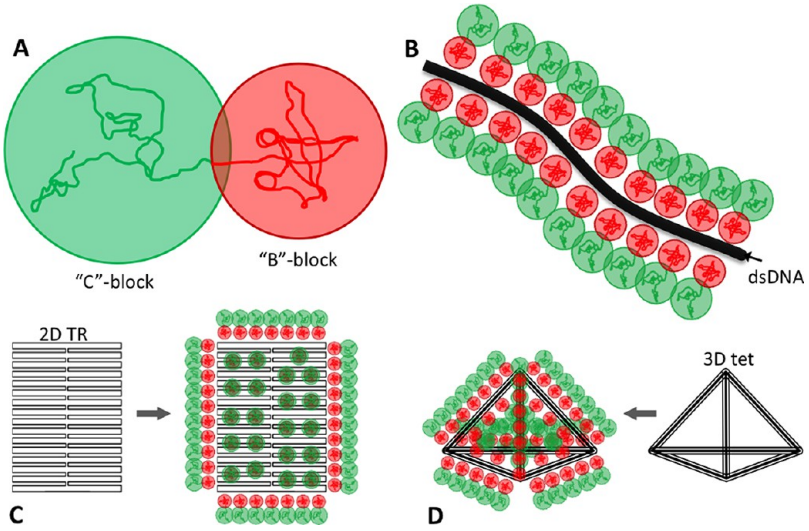

Figure 1. Schematics of engineered diblock polypeptides and their interactions with DNA. (A) Schematic of an engineered diblock polypeptide containing a compatibilizing "C"-block (green) and a binding "B"-block (red). (B) Schematic of diblock polypeptides bound at nonspecific locations to dsDNA (black). (C) Schematic of diblock polypeptides nonspecifically bound to a 2D DNA origami known as TR or "tall rectangle". (D) Schematic of diblock polypeptides bound to a 3D tetrahedral DNA origami.

notoriously difficult to dissociate from one another and to suspend as individual tubes rather than clusters.[11,12] There is a clear need for understanding and optimizing solution conditions such that they are compatible with all assembly components. This is especially true if larger macromolecular assemblies are to be formed and maintained over significant periods of time as well as where high concentrations of components (~10 μM) are needed, as is the case when forming networks or gels. Thus, there is a need for investigation of viable compatibilizing agents in order to advance DNA-based nanotechnology beyond its current state as a promising bottom-up self-assembly technique and establish it as a reliable fabrication technology for biomedical, optical, or electronics industries. Compatibilizing agents will allow desired supramolecular complexes to exist stably in solution for longer periods of time and will provide vastly improved assembly yields. Taking inspiration from biology, which makes use of many soluble proteins to bind, coat, and stabilize molecular species with low water solubility, we here examine the use of diblock proteins that have been specifically designed for binding to and solubilizing DNA and DNA-functionalized nanomaterials.

Previous studies have developed "protein-based polymers" (or protein polymers, for short), including block polypeptides and other engineered modular proteins, for a variety of purposes.[13−23] Specifically, we have previously developed protein polymers that can coat DNA and DNA structures such as DNA origami[24−26] and protein polymers that can mimick the coassembly of viral capsid proteins such as the Tobacco Mosaic Virus capsid protein, with their nucleic acid templates.[25] One of the applications of the protein polymers that were developed to coat DNA structures is to serve as compatibilizing agents, in the sense described above, by binding and coating two or more unlike constituents such that they become amenable to common solution conditions. This is the application that we will investigate here in more detail.

Two previously described diblock proteins will be considered here: one denoted by C_4−B^{K12},[24,28] and one denoted by C_8−B^{Sso7d}.[26,29−34] Both feature a hydrophilic "C" block that forms random coils in solution, and a "B" block that binds nucleic acids. The hydrophilic block increases the solubility of its bound constituents and hence acts as a compatibilizing block. The amino acid sequence of one unit of the hydrophilic block is $C_1 = (GXY)_{33}$, with a glycine every third residue like in collagen. However, by choosing amino acids that are much more hydrophilic than in natural collagen for the X and Y positions, these polymers form random coils rather than triple helices.[27] The nature of the binding block, "B," can be tailored for specific applications. Here we use two different DNA binding blocks. The dodecalysine binding block B^{K12} binds through nonspecific electrostatic interactions and will bind not only to DNA but also to any sufficiently highly negatively charged object. The B^{Sso7d} binding block is composed of a small (7 kDa) basic protein from the thermophilic archaeon *Sulfolobus solfataricus*, named Sso7d. This is a very well-characterized and very stable protein that binds specifically to DNA, without any preference for a certain DNA sequence.[26,29−34] A schematic of the diblocks themselves and their mode of binding to DNA, two- and three-dimensional (2D and 3D) DNA origami, is shown in Figure 1.

These diblock proteins may act as compatibilizing agents for nanostructures made not only from DNA but also other materials such as AuNPs or carbon nanotubes and therefore hold promise to act as a synthetic surfactant, protecting and compatibilizing multiple components, allowing them to remain in salty solutions for longer periods of time and making them more likely to find their lowest energy, thermodynamic equilibrium conformations. We have performed preliminary examinations of the interactions of these diblocks with single-stranded DNA (ssDNA) and dsDNA and with one DNA origami nanostructure,[24−26] but an examination of the interaction with other DNA origami structures, and an examination of the further interactions of the diblocks when other nanocomponents such as AuNPs are also present, has not yet been done. This is the purpose of the present paper.

In order to characterize the compatibilizing effect of the diblocks when other nanocomponents are also present, we will use two different DNA origami designs with contrasting

DOI: 10.1021/acsnano.6b07291
ACS Nano 2017, 11, 831−842

geometric properties. One of these structures is Rothemund's original "tall rectangle",[3] a 2D, planar structure that binds to substrate surfaces with very high contact surface area, occluding a large amount of the origami's surface area from the surrounding aqueous solution. Preliminary investigations of the interactions of the diblocks and tall rectangle origami have been outlined.[26] In contrast, diblock polypeptides interactions with 3D wireframe origami structures[35−40] have not previously been examined. An origami structure was specifically designed for this study; it is a 3D, tetrahedral wireframe structure, which, when bound to substrate, maintains only a relatively small portion of its surface area in contact with the substrate (further design details can be found in the Supporting Information). Herein, we will investigate the amount of compatibilizing proteins required to saturate the 2D rectangular and our 3D tetrahedral origami structures and explore their surface-dependent solubilization parameters. We also examined the degree of protection from enzymatic digestion afforded by the bound diblocks by monitoring the survival time of complexed DNA origami following exposure to DNase I, a nonsequence-specific endonuclease. Next, we explored the diblocks' capacity for maintaining the solubility of DNA-coated gold nanospheres (AuNS) and gold nanorods (AuNR) at elevated salt concentrations when protected by the proteins. Finally, assembly reactions between diblock-compatibilized DNA origami and diblock-compatibilized, DNA-functionalized AuNS were examined to ensure that the compatibilizing proteins do not interfere with the molecular recognition aspects of the system. We find that both proteins examined protect 2D and 3D DNA origami structures from enzymatic degradation and compatibilize DNA and DNA-functionalized AuNPs, widening the range of salt concentrations at which the DNA origami and AuNPs may coexist, showing that these diblock polypeptides promote the formation of desired organic/inorganic assemblies. Additionally, we find that these diblocks enable a time-dependent, protein-assisted, surface desorption process that can be rate-controlled based on different DNA origami shapes. This desorption process could find use in the realm of time-released drugs, where origami carrying medicinal cargo could be solubilized at different rates and thus become bioavailable with different temporal profiles.

RESULTS/DISCUSSION

Tetrahedral Origami Design and Production. A variety of 2D and 3D nanostructures have been engineered from DNA origami, with a broad range of geometries.[41,42] Most of the 3D structures have been bulk structures, though some wireframe structures exist,[35−40] and due to size limitations of DNA scaffolds, the size of existing 3D structures has been fairly limited[37,43−47] In order to create a structure useful in many types of experiments, from chiral and optical experiments to creating the building blocks for nanoelectronic circuitry production, we designed a wire-frame DNA tetrahedron large enough to allow for independent programming of materials onto each arm and vertex. In particular, we ensured that the structure could accommodate a nanorod (up to 50 nm in length) per edge and a nanoparticle (up to 25 nm in diameter) per vertex (Figure 2). Note that while other DNA tetrahedra exist,[48−60] none are as large as those designed herein, and thus none of the previously published tetrahedra are capable of accommodating our nanorods (or other large aspect ratio objects).

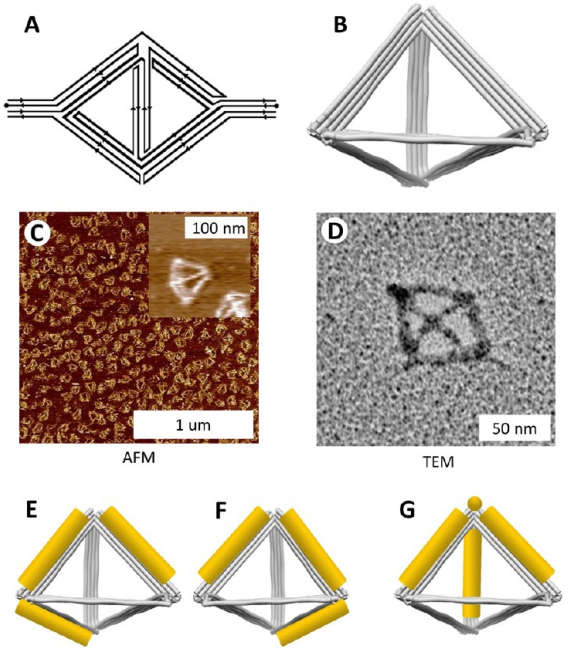

Figure 2. (A) 2D rendering of 3D tetrahedral M13mp18 scaffold routing map with four-helixwide "arms". The left and right sides of the diagram, when connected, represent the structure in 3D. (B) 3D model from CanDo simulation of tetrahedral DNA origami, designed using caDNAno. (C) Wide-field AFM of experimentally realized tetrahedra and inset close-up of an individual tetrahedron. (D) Uranium-stained TEM of tetrahedron. (E) A left-handed and (F) right-handed chiral nanostructure, and (G) schematic of a nanostructure with the core architecture of a 3D single-electron transistor.

We designed a 3D wireframe tetrahedron comprised of a similar number of base pairs as the 2D planar tall rectangle origami, but with a smaller area of occluded nucleotides (larger solvent-exposed surface area) and a smaller contact area binding with a substrate surface. A 2D representation of the 3D scaffold routing map of the DNA origami is shown in Figure 2A. Each arm of the tetrahedron is comprised of four helices of dsDNA, and designed staples hold the scaffold in the desired conformation. The route of the scaffold trace through the target structure was chosen so as to minimize the risk of tangling (*i.e.*, scaffold forms no knots and avoids crossing itself). The scaffold routing map was incorporated into 3D design within the DNA origami design program, caDNAno,[61] and DNA staple strand sequences were generated to hold the scaffold in the desired conformation. For further details of the design, see the Supporting Information. A predicted final 3D structure of scaffold and staples was produced using CanDo[62−64] and is shown in Figure 2B.

Scaffold and staples (1:10) were slowly annealed through the melting temperature range of DNA (from 80 to 20 °C over 2 h) and imaged *via* transmission electron microscopy (TEM) and atomic force microscopy (AFM), as shown in Figure 2C,D, respectively.

These DNA structures can be utilized to programmably template the self-assembly of other components, such as AuNPs. This can be accomplished by extending certain staple strands at desired sites with chosen DNA sequences, such that the extended ssDNA become binding sites to a target assembly of nanocargo bearing complementary ssDNA. Example

DOI: 10.1021/acsnano.6b07291
ACS Nano 2017, 11, 831−842

conformations, chiral and transistor structures, are shown in Figure 2E–G.

Binding Properties of Diblock Proteins and Tetrahedral DNA Origami. To examine the stoichiometry with which the tetrahedral DNA origami becomes coated with different candidate protein compatibilizers, aliquots of DNA tetrahedra were mixed with varying amounts of C_4–B^{K12} or C_8–B^{Sso7d} in order to obtain various protein/bp ratios, as can be seen in Figure 3. Samples were incubated at various ratios of molecules

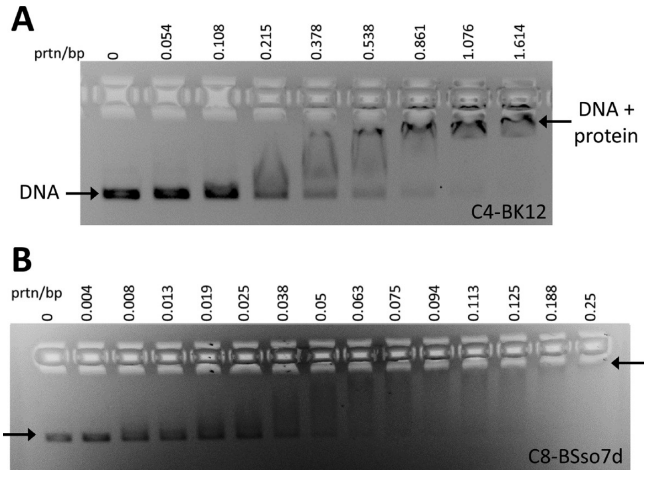

Figure 3. Electrophoretic mobility shift assay for 5.4 kbp tetrahedral DNA origami complexed with (A) C_4–B^{K12} and (B) C_8–B^{Sso7d}. Each lane contains ~100 ng of DNA. Protein/DNA bp ratios are given above each lane.

of protein to base pairs of DNA (protein/bp ratios from 0 to 1.614) and were subjected to agarose gel electrophoresis to determine the saturation point at which the origamis were fully coated in protein. Similar to the tall rectangle results previously reported,[26] a clear inflection point can be seen, indicating the point at which the DNA becomes saturated with protein. For the C_4–B^{K12} protein, the DNA origami began to experience a change in net charge due to the positive nature of the protein; this, as well as an increase in the overall size of the complexes, caused them to migrate more slowly in the gel starting at a protein/bp ratio of 0.108 and became fully saturated with protein around a protein/bp ratio of between 0.86 and 1.08. A similar trend was observed for DNA origami mixed with the C_8–B^{Sso7d} protein, however, the migration changes occurred at much lower protein/bp ratios. The decrease in migration rate began around 0.013 and appeared to saturate around 0.125 protein/bp. This difference in mobility shift and protein/bp stoichiometry between the two proteins likely arises due to the high binding affinity and specificity for DNA that the Sso7d domain imparts, requiring less protein to saturate the DNA than with the nonspecific K12 binding domain.

AFM Imaging of Protein-Coated Tetrahedral DNA Origami. To examine the final structure of origami–protein complexes, AFM was performed at various protein/bp ratios. Normally, DNA origami is imaged on mica under 1×TAEMg buffer (40 mM Tris, 20 mM acetic acid, 1 mM EDTA, 12.5 mM magnesium acetate), during which the Mg^{2+} ions act to electrostatically bridge between the negatively charged mica substrate and the negatively charged phosphates along the DNA backbone, thereby conveniently anchoring the origami to the substrate for imaging. For DNA origami samples that have been complexed with a diblock protein, the presence of the protein brings the net charge on the supramolecular complex to neutral or positive, and thus the samples are unlikely to be electrostatically attracted to a positively charged Mg^{2+} layer. As such, in this experiment, the positively charged Mg^{2+} layer was decreased by diluting 10-fold with DI H_2O prior to pipetting the protein-DNA sample onto mica, then the sample dried under a brief stream of nitrogen.

AFM of these samples showed interesting results. Control samples of DNA origami at 0 protein/bp and in 10-fold diluted TAEMg, being negatively charged, did not bind to mica. However, with even low concentrations of protein, below the saturation point seen in the gel images of Figure 3, the origami–protein complexes bound to the negatively charged mica. Figure 4 shows dry AFM and corresponding height maps

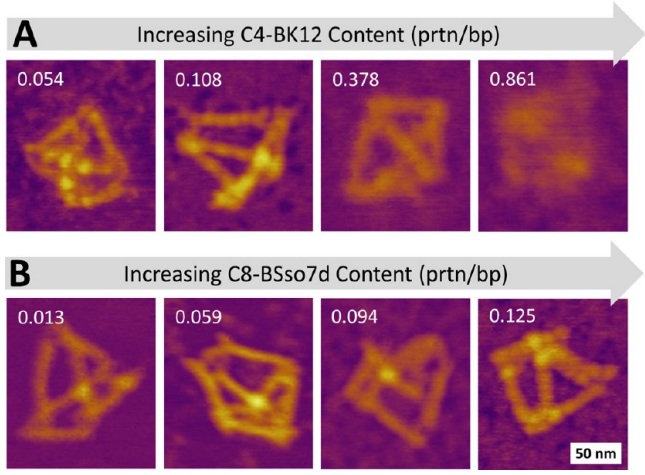

Figure 4. (A) AFM images of tetrahedral DNA origami complexed with C_4–B^{K12} at different protein/bp ratios (indicated in the upper left corner of each panel). (B) Corresponding AFM of origami complexed with C_8–B^{Sso7d} at different protein/bp ratios as indicated on each panel. The scale bar is 50 nm.

of tetrahedral DNA origami–protein complexes for each of the two diblock proteins at various protein/bp ratios. Similar to results shown in ref 26, at high protein concentrations, the texture of the DNA origami becomes markedly different. For complexes containing the C_4–B^{K12} protein, the saturation point occurs at protein concentrations high enough to alter the texture of the DNA origami, whereas the lower saturation point associated with the C_8–B^{Sso7d} complexes allows for the existence of saturated DNA–protein complexes that remain unaltered in shape and texture. The cause of the high saturation point for the C_4–B^{K12} protein is likely due to the nonspecific, electrostatic nature of the B^{K12} domain binding, which strongly interacts along the sugar-phosphate backbone of the DNA and changes or possibly disturbs the precise spacing of nucleotides of the DNA helices. It is also possible that the B^{K12} domain competes with Mg^{2+} cations, which are responsible for the formation of Holliday junctions necessary for folding of the DNA origami. If the Mg^{2+} ions are replaced by protein, the Holliday junctions could be destabilized or distorted. Conversely, the DNA-specific binding of the B^{Sso7d} domain in the C_8–B^{Sso7d} protein appears not to disturb the structure of either origami shape, even at high protein/bp ratios where the origamis are saturated with protein, and may even help preserve the structure's form. It is possible that the C_8–B^{Sso7d} protein

DOI: 10.1021/acsnano.6b07291
ACS Nano 2017, 11, 831–842

binds without displacing Mg^{2+}, however, further experiments will be needed to clarify this point.

Protection against Enzymatic Degradation of Protein-Coated Tetrahedral DNA Origami. The degree of sequestration of DNA molecules coated with diblock protein is relevant for a variety of possible applications, from the accessibility of ssDNA tags, which attract/bind complementary strands, free in solution or bound to nanocargo, to the viability of utilizing these complexes *in vivo*. In this experiment, tetrahedral DNA origami (annealed with 10× excess staple strands) were incubated with each of the diblock proteins and exposed to DNase I (a nonsequence-specific endonuclease) for varying periods of time. Aliquots were removed at chosen time points, the nuclease degradation was quenched by EDTA, and subsequently the samples were examined by agarose gel electrophoretic mobility shift assay.

Results from this experiment include a set of control samples with no protein protection as well as sets of samples protected by C_4–B^{K12} or C_8–B^{Sso7d} (Figure 5). Unprotected DNA

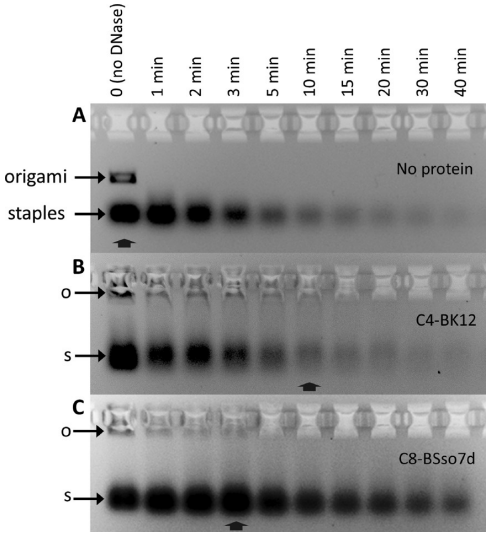

Figure 5. Nuclease protection assay of tetrahedral origami (A) without protein protection, (B) complexed with C_4–B^{K12} (0.861 protein/bp), and (C) complexed with C_8–B^{Sso7d} (0.188 ptn/bp). Samples were incubated with DNase I, and reaction aliquots were quenched with EDTA at different times. Aliquots were run in an agarose gel and stained with ethidium bromide. Nuclease incubation times in minutes are indicated above the lanes. Arrows below the lanes indicate the longest-lasting evidence of origami.

origami is negatively charged and thus readily migrates into the gel, whereas the DNA–protein complexes are large and approximately charge neutral and thus migrate only slightly into the gel. The dsDNA band in the unprotected sample is visible for <1 min of incubation with enzyme, whereas the DNA–protein complexes maintain a dsDNA band for 3 min (with 0.188 C_8–B^{Sso7d} protein/bp) and 10 min (with 0.861 C_4–B^{K12} protein/bp), indicating that both proteins protect DNA from enzymatic digestion compared to unprotected. Likewise, the protein-protected samples maintain stronger ssDNA bands (staple strands) as incubation times are increased, especially with C_8–B^{Sso7d}, indicating that the C_8–B^{Sso7d} more strongly protects ssDNA than the C_4–B^{K12} protein does. This explains the lighter ssDNA bands for the sample without protein protection in Figure 5A. The nuclease is able to digest more DNA, both dsDNA as well as ssDNA, in a given period of time when no protein protection is present. A similar experiment was performed using tall rectangle origami with 0.09 U DNase rather than 0.4 U DNase, such that the reaction proceeded at a lower rate (see Figure S3). This experiment confirmed the extended lifetime of protein-protected origami and more precisely determined origami lifetimes due to the reduced degradation rate. This nuclease protection may be attributed to steric repulsion from the large brush-like structure that the protein forms around the DNA.[26] Of course, this coating could also have an effect on the hybridization ability of protein-protected DNA origami and DNA-AuNPs; this hypothesis will be tested below. The nuclease protection result is promising in terms of utilizing these complexes *in situ*, as these proteins appear to decrease the enzymatic accessibility of the DNA origami to digestive DNases.

Solubilization and Surface Release Analysis of two DNA Origami Shapes. In the previous sections, AFM and the gel mobility of tetrahedral origami were studied and compared to the observations previously published for tall rectangle DNA origami. In this section and in ensuing sections, experiments are described in which neither tall rectangle nor tetrahedra have been explored before, and thus interactions with both are reported.

The two types of DNA origami, each with different surface areas available for binding to substrate, were landed on a mica surface in 1×TAEMg buffer. After protein addition, the samples were imaged by AFM, and origami solubilization (*i.e.*, release from the mica surface) was observed and related to the differing contact areas between DNA and mica.

The two types of DNA origami, tall rectangle and tetrahedra, were mixed together in their native 1×TAEMg, pipetted onto a freshly cleaved mica surface, and imaged *via* wet AFM. After adding a given amount of diblock protein and imaging by AFM every few minutes, the tetrahedral origami was noticeably solubilized and released from the surface more rapidly than the tall rectangle origami, regardless of protein type. The control sample in which no protein was added showed that both types of origami remained bound after 2 h, indicating that the addition of the protein was the cause of the release. This interesting result implies that the selective properties of the DNA-protein association may be useful and controllable. AFM images from the control are shown in Figure 6A, with the addition of C_4–B^{K12} in Figure 6B and with C_8–B^{Sso7d} in Figure 6C. Additional time points for the C_8–B^{Sso7d} sample are available in Figure S2.

A rough calculation of the contact surface area of tall rectangle on the substrate gives a value of 4736 nm^2, whereas the surface area of a tetrahedron on the substrate is calculated as 1236 nm^2. The lower surface contact area for tetrahedron likely makes it easier to remove from the surface as well as leaving a much larger solvent exposed surface area for protein binding and solubilization. Likewise, the contact perimeter of the tall rectangle on the substrate is calculated to be 276 nm, whereas the contact perimeter of the tetrahedron is calculated as 357 nm. The larger contact perimeter of the tetrahedron provides more access to the incoming, solubilizing protein and is likely another reason that the tetrahedron is lifted first.

Possible applications for this time-dependent, protein-assisted DNA desorption include the implementation of time-released drugs, where origami carrying medicinal cargo could be solubilized at different rates and thus absorbed by a patient with different temporal profiles. The different types of origami could even carry different medicines. We imagine a pill, perhaps

DOI: 10.1021/acsnano.6b07291
ACS Nano 2017, 11, 831–842

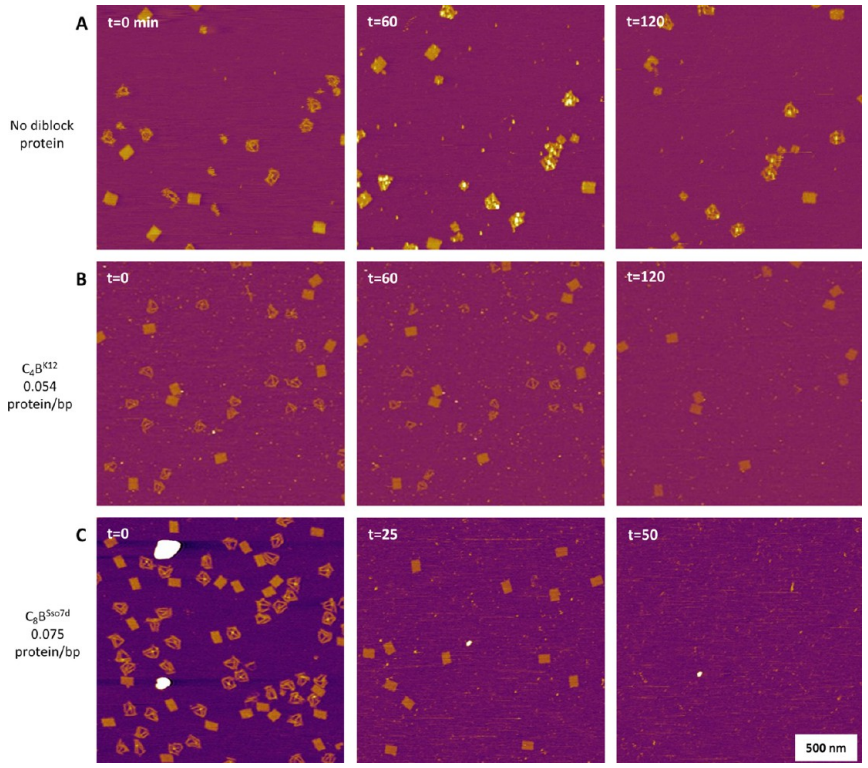

Figure 6. (A) Tall rectangle and tetrahedral DNA origami in 1×TAEMg, bound to mica surface and imaged over time. From left to right, panels show the origami imaged after 0, 60, and 120 min. All origamis remain bound. A small amount of AFM drift is noted between the t = 0 and t = 60 min images, but does not affect the sample. (B) Mixed origami in 1×TAEMg, bound to a mica surface, where, at time zero, the C_4−B^{K12} protein was added to bring the solution to 0.059 protein/bp, and imaged over time. From left to right, panels show the origami imaged after 0, 60, and 120 min. At 120 min, only the tall rectangle origami remain bound to the mica. (C) Mixed origami in 1×TAEMg, bound to a mica surface, where, at time zero, the C_8−B^{Sso7d} protein was added to bring the solution to 0.075 protein/bp, and imaged over time. From left to right, panels show the origami imaged after 0, 25, and 50 min. After 25 min, only the tall rectangle origami remained bound to the mica surface. After 50 min, no DNA origami remained on the surface. It is of note that these images were taken of the same area; the visible changes are due to actual changes within the sample and not due to tracking of different areas.

containing mesoporous silica, with bound DNA origami-medicinal cargo as well as the protein, such that upon ingestion and rehydration, the protein and origami would reconstitute, and the release process would be initiated. Another possible application for protein-assisted DNA desorption could be the reversible binding, and collection, methods such as in refs 65 and 66.

Annealing Origami in the Presence of Protein. To investigate whether DNA-binding proteins assist or inhibit assembly of origami, protein was added to the pool of ssDNA staples and scaffold, which were then annealed by slow cooling to allow dsDNA and origami formation. Under normal solution conditions, a fairly high Mg^{2+} concentration (12.5 mM) is required to allow formation of Holliday junctions and DNA origami. This experiment explores DNA assembly behavior in the presence of protein compatibilizers under normal and reduced [Mg^{2+}] conditions. Tall rectangle origami was mixed with either C_4−B^{K12} or C_8−B^{Sso7d} in either 2, 6 , or 12.5 mM Mg^{2+}, at protein concentrations below, at, or above the saturating concentration, annealed from 80 to 20 °C over 2 h, and then imaged *via* AFM in air (as described in the Methods/Experimental section).

For each protein and protein concentration, origami−protein complexes were able to properly form at the regular [Mg^{2+}] of 12.5 mM, (Figures 7 and 8, rightmost columns) producing images similar to those for samples where protein was added after origami formation. This indicates that the presence of diblock protein in solution during annealing does not hinder the Holliday junction or origami formation. At a lower [Mg^{2+}] in which origami does not usually form (6 mM Mg^{2+}), the presence of low to moderate amounts of diblock protein allows origami formation. With C_4−B^{K12}, a moderate amount of protein is required to allow for origami formation, whereas with C_8−B^{Sso7d}, only a small amount of protein is required for origami formation, likely due to the specific nature of the Sso7d binding domain (Figures 7 and 8, middle columns). The decrease in Mg^{2+} concentration in the presence of diblock protein will increase the efficiency of later processing steps involving metal nanoparticles by decreasing nanoparticle aggregation. These experiments also confirm the thermal stability or resilience of the diblock proteins up to 80 °C, as it is clear that they still promote DNA origami stability after having been heated during the annealing process.

Stabilization of Preformed Origami. It was shown that these diblock proteins protect already formed origami and allow origami to anneal from ssDNA. This section investigates what happens when two types of origami, each designed using the same scaffold sequence, are combined in solution. Hybridization of complementary oligonucleotides is dynamic, and thus staples have a binding and release rate. If only one set of staples, for a particular design, is included in a mixture, these on and off reactions can be ignored, since they always result in reformation of the same origami design. However, when two or more disparate origami structures who share the same scaffold strand

DOI: 10.1021/acsnano.6b07291
ACS Nano 2017, 11, 831−842

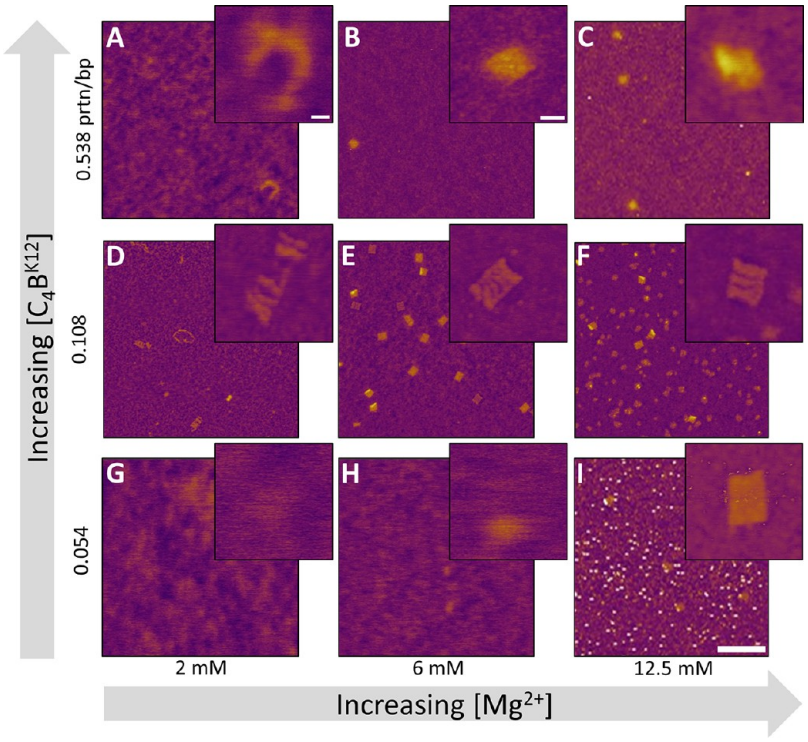

Figure 7. Tall rectangle origami annealed in varying amounts of C_4–B^{K12} protein and TAEMg buffer. (A) 0.538 protein/bp, 2 mM Mg^{2+}; (B) 0.538 protein/bp, 6 mM Mg^{2+}; (C) 0.538 protein/bp, 12.5 mM Mg^{2+}; (D) 0.108 protein/bp, 2 mM Mg^{2+}; (E) 0.108 protein/bp, 6 mM Mg^{2+}; (F) 0.108 protein/bp, 12.5 mM Mg^{2+}; (G) 0.054 protein/bp, 2 mM Mg^{2+}; (H) 0.054 protein/bp, 6 mM Mg^{2+}; and (I) 0.054 protein/bp, 12.5 mM Mg^{2+}. Large scan area scale bar is 500 nm. Inset scale bar is 50 nm.

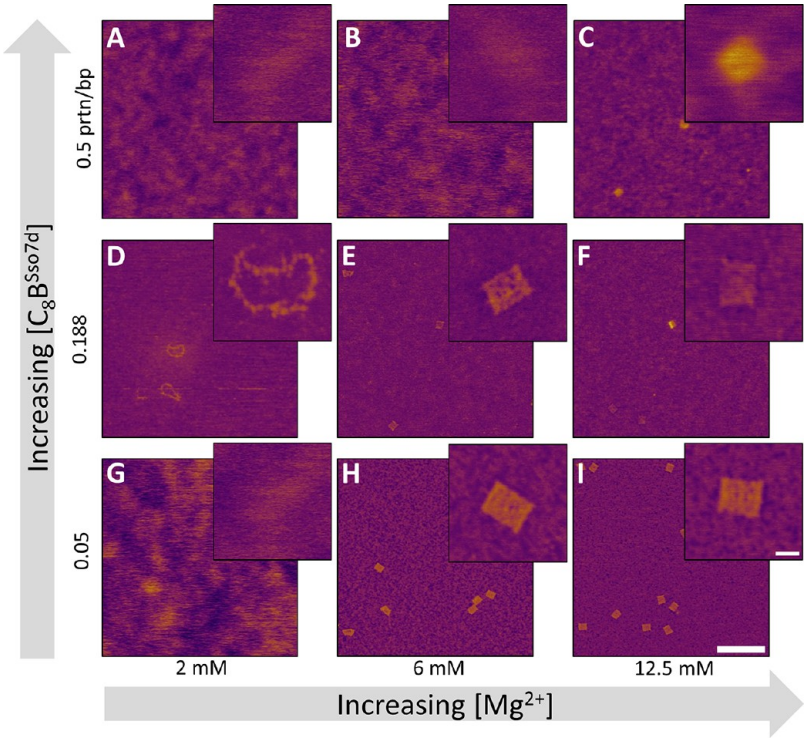

Figure 8. Tall rectangle origami annealed in varying amounts of C_8–B^{Sso7d} protein and TAEMg buffer. (A) 0.5 protein/bp, 2 mM Mg^{2+}; (B) 0.5 protein/bp, 6 mM Mg^{2+}; (C) 0.5 protein/bp, 12.5 mM Mg^{2+}; (D) 0.188 protein/bp, 2 mM Mg^{2+}; (E) 0.188 protein/bp, 6 mMMg^{2+}; (F) 0.188 protein/bp, 12.5 mM Mg^{2+}; (G) 0.05 protein/bp, 2 mMMg^{2+}; (H) 0.05 protein/bp, 6 mMMg^{2+}; and (I) 0.05 protein/bp, 12.5 mM Mg^{2+}. Large scan area scale bar is 500 nm. Inset scale bar is 50 nm.

sequence are mixed (in the absence of excess staple strands) and left at room temperature for 4 days, rehybridization, or strand exchange, is allowed to take place, and the final structures formed may be different than any of the designs.

DOI: 10.1021/acsnano.6b07291
ACS Nano 2017, 11, 831–842

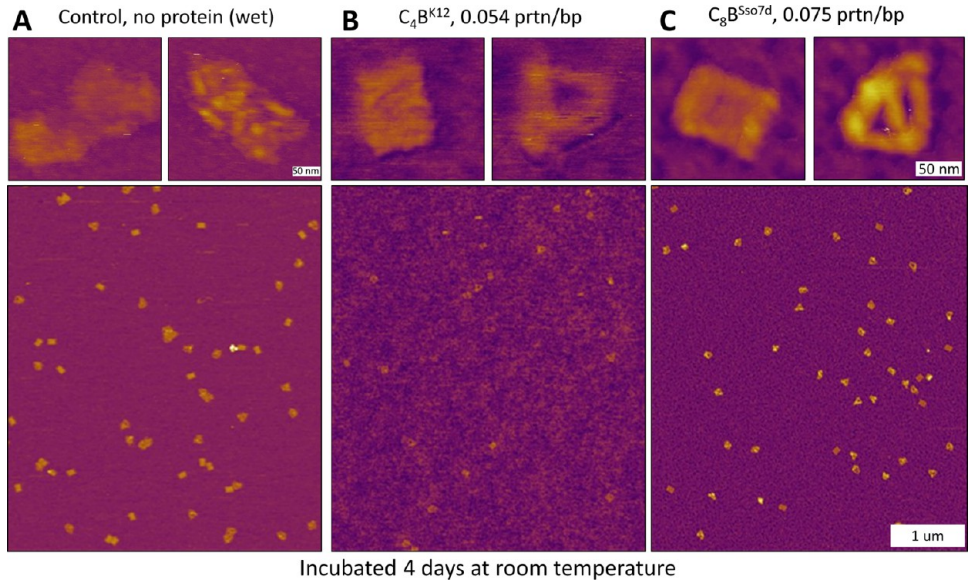

Figure 9. AFM of mixed tall rectangle and tetrahedral origamis after 4 days of incubation at room temperature in 1×TAEMg containing (A) no protein, (B) C_4–B^{K12} at 0.054 protein/bp, or (C) C_8–B^{Sso7d} at 0.075 protein/bp.

Results show (Figure 9) that without diblock protein protection, large mixed and partially folded structures are formed, while in the presence of either diblock, only the expected rectangle or tetrahedral origami is observed. When protected by the protein, the origami structures are less likely to exhibit strand-exchange behaviors and hybrid structure formation; they remain much more intact compared to unprotected origami mixtures.

This protection can allow more complicated and cooperative network structures, involving multiple DNA origami types. Manipulating this behavior with carefully designed structures could also yield useful transformations over designed time periods.

Protein-Assisted Stabilization of DNA-Functionalized AuNPs in High Salt Concentrations. The next experiment was designed to test if the diblocks are able to protect AuNPs from high salt concentrations in which they typically aggregate and precipitate. DNA-functionalized AuNPs were mixed with C_8–B^{Sso7d}, subsequently exposed to high Mg^{2+} concentrations, and compared *via* UV–vis absorbance spectroscopy to the behavior of AuNPs without protein protection. A decrease in absorbance was observed after Mg acetate addition for unprotected AuNPs due to nanoparticle aggregation, whereas DNA–protein complexed AuNPs do not show a decrease in absorbance after addition of Mg acetate. This is indicative of protein protection and thus the solubilization of AuNPs, so that they are capable of existing in a wider variety of solution conditions and therefore will remain in solution for longer periods of time within which they can assemble into their lowest-energy configurations. Results of this experiment with AuNSs are shown in Figure 10A and with AuNRs in Figure 10B.

Analysis of DNA Origami-AuNS Hybridization in the Presence of Protein Compatibilizers. To test the ability of protein-protected DNA-AuNSs to bind with the complementary sequence displayed on the protein-protected DNA origami (*i.e.*, to ensure that single-stranded tags remain capable of hybridization), a control sample without protein and a protein-protected sample were simultaneously mixed, in each case, with the same number of moles of tall rectangle origamis of each and also the same number of moles of AuNSs in each sample (where the number of AuNSs is 5 times the number of binding sites in order to bias the system toward origami binding sites fully saturated with AuNSs). The C_8–B^{Sso7d} protein was used for this experiment, since it produced less distortion of origami than the C_4–B^{K12} protein. A concentration of C_8–B^{Sso7d} protein equivalent to 0.188 protein/bp was used, since this concentration is the lowest point at which the protein appears to saturate the DNA. Control and protein-protected samples were incubated at room temperature overnight and then heated to 37 °C for 20 min to promote hybridization before being incubated on mica and imaged dry (Figure 11).

Both samples revealed high yields of AuNS binding at target sites, with the control sample (90.7% of binding sites occupied) beating the protein-containing sample (78.5% of site occupied) in terms of site saturation. However, the control sample was mostly comprised of clusters of origami, where AuNSs were shared between two or more origamis, while the protein-protected sample contained almost no clusters (Figure 11D), and thus the actual yield of desired product (one origami with one AuNS at each corner) was higher for the protein-containing sample (31.8%) than for the control (18.9%). To ensure statistical significance, over 100 origamis were analyzed for each sample. Example images from this experiment are shown in Figure 11B,C. Additional images used for statistical analysis are shown in Figure S5.

To confirm that the clusters in the control were not formed due to the dilution of the 1×TAEMg buffer during incubation on mica, an experiment was performed in which the sample was incubated on mica in 1×TAEMg (Figure S6). Furthermore, electrophoresis of these samples was performed to further analyze the interactions of the system's components (Figure S4). Due to difficulties imaging a 3D wireframe origami on a 2D surface, this experiment has not been performed with tetrahedral origami, however, based on these tall rectangle results, the principles should transfer to other origami shapes. Better imaging technology such as *in situ* fluid TEM could make analysis of this experiment possible.

DOI: 10.1021/acsnano.6b07291
ACS Nano 2017, 11, 831–842

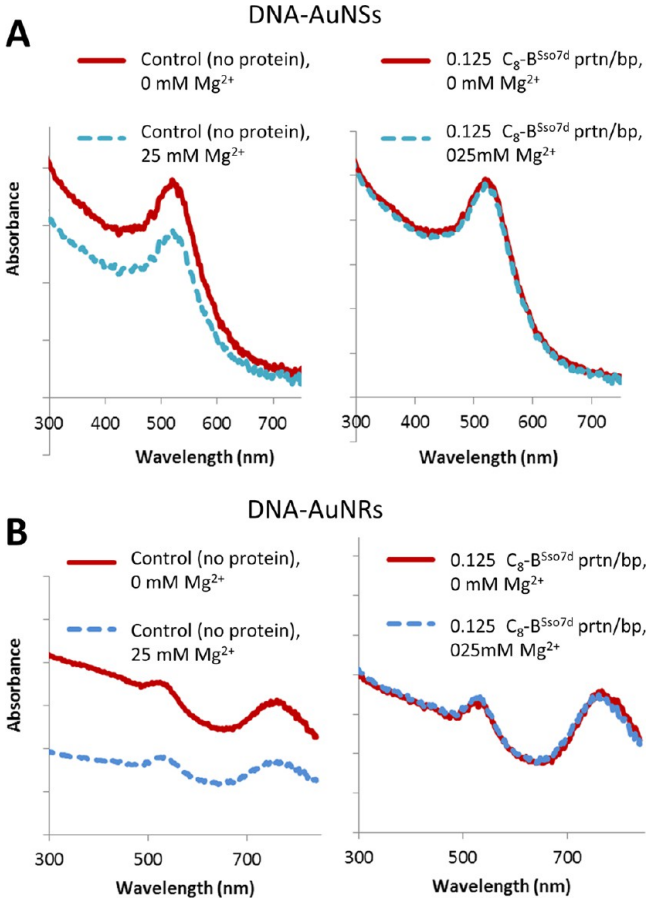

Figure 10. (A) (Left) DNA-AuNS control without protein and (right) DNA-AuNSs with 0.125 C_8−B^{Sso7d} protein/bp before (red, solid lines) and 2 h after (blue, dotted lines) exposure to 25 mM Mg acetate. (B) (Left) DNA-AuNR control without protein and (right) DNA-AuNRs with 0.125 C_8−B^{Sso7d} protein/bp before (red, solid lines) and 2 h after (blue, dotted lines) exposure to 25 mM Mg acetate. For each (A and B), the control shows a drop in absorbance after Mg^{2+} addition, whereas the protein-protected sample does not exhibit a drop in absorbance.

CONCLUSIONS

The application of polypeptides as compatibilizers of 2D and 3D DNA origami has been explored and developed here. Compatibilizing diblock proteins have been added to origami postassembly as well as during the assembly process. They have been shown to protect DNA from nucleases, protect AuNPs from aggregation due to high salt concentrations, and assist the assembly of DNA origami−AuNS complexes in desired, individual forms rather than in undesired clusters. Stabilization of multiple types of origami in solution by protecting against exchange of staples was also demonstrated. In addition, the diblock proteins have been shown to differentially solubilize and release different origami structures from a surface based on differences in contact surface areas, which may find use in biomedical applications. Overall, the C_8−B^{Sso7d} protein appears most suitable in that saturation occurs at a lower protein/bp ratio and avoids distortion of the origami. As such, it seems to be the best candidate to explore for further testing and development.

The modularity of these diblock polypeptides should allow the DNA-binding block to be exchanged for other binding blocks, for example, a carbon nanotube-binding peptide[69] such that other desired components could be solubilized and compatibilized for assembly of diverse supramolecular complexes. The aim is to expand bionanomanufacturing strategies for solution-phase fabrication of photonic and electronic devices, since biomanufacturing is inherently more sustainable and "green" due to its decreased reliance on rare earth elements as well as process facilities are many orders of magnitude less expensive to construct and run than conventional microlithography facilities.

METHODS/EXPERIMENTAL

Materials. M13mp18 single-stranded DNA 7249 nt (ssDNA) was purchased from New England Biolabs (Ipswich, MA, USA). All short ssDNA staples used for DNA origami formation and thiolated captures strands were purchased from IDT (Integrated DNA Technologies, Inc.). The sequences of staples and the scaffold/staple layout for the tall rectangle design can be found in ref 3. Sequences for staples and the scaffold/staple layout for the 3D wireframe tetrahedron can be found in the Supporting Information. Centrifuge filter units were purchased from Millipore (Microcon-30 kDa Centrifugal Filter Units). Citrate-stabilized AuNPs, herein called AuNSs (5 nm, British Biocell International) and bis(*p*-sulfonatophenyl)phenylphosphine (BSPP) were purchased from Sigma-Aldrich. AuNRs were synthesized following the first growth step of the previously described procedure.[70] TCEP was purchased from ThermoFisher Scientific. Freeze 'N Squeeze columns were purchased from BioRad Laboratories. Electrophoresis was performed using Agarose A purchased from Bio Basic Inc. EtBr nucleic acid stain was purchased from Genesee Scientific. Bovine pancreas DNase I lyophilized powder was purchased from Roche Applied Science (Mannheim, Germany). Proteins C_4B^{K12} and C_8−B^{Sso7d} were produced and purified following previously published methods[25,71] and provided by the authors of ref 24.

Preparation of DNA Origami. To assemble the DNA origami, 100 μL of solution were prepared such that the final solution is comprised of 5 nM single-stranded M13mp18 DNA scaffold, 50 nM single-stranded DNA staple strands, and 1×TAEMg. The solution was heated to 80 °C and then cooled to 20 °C over 2 h and subsequently kept at 4 °C. Removal of excess ssDNA was accomplished by centrifuge filtration using Microcon Centrifuge Filters, centrifuged at 2400 *g* for 2 min, and repeated 4 times.

Preparation of DNA-Coated AuNSs. Following the recipe of refs 67, 72, and 73, 3 mg of BSPP was added to 10 mL of purchased AuNS solution. After 48 h of incubation, the AuNSs were concentrated by adding ∼260 mg of NaCl until the solution changed from red to slightly purple and centrifuged for 30 min at 800 *g*. In the meantime, thiol-modified DNA capture sequences were reduced by mixing thiol-DNA with TCEP-coated styrene beads in 0.75×TE buffer and rotated to mix for 1 h. After centrifuging the AuNS/BSPP/NaCl solution, the supernatant was removed without disturbing the visible Au pellet. 200 μL of BSPP solution (3 mg BSPP in 10 mL DI H_2O) was added, followed by 200 μL methanol, after which the solution was centrifuged a second time for 30 min at 800 *g*. The supernatant was again removed, and the AuNSs were resuspended in the same BSPP solution to a total volume of 200 μL. The now-reduced, thiol-modified DNA sequence was then centrifuged at 500 *g* for 2 min to separate the DNA from the styrene beads. The clear supernatant containing the thiol-DNA was pipetted and added to the AuNS solution, at which time the buffer was adjusted to 1×TAE/50 mM NaCl. After 48 h of incubation, thiolated T_5 strands were added at a Au:T_5 ratio of 1:60 to fully backfill the AuNS-DNA conjugates and again incubated for 48 h. Excess DNA strands were removed from the AuNS-DNA conjugates by running the conjugate solution on a 3% agarose gel (1×TAE) for 20 min, at 10 V/cm. The AuNS-conjugate band was extracted by cutting out the band of interest, squishing it with a flat surface, and centrifuging it using a Freeze 'N Squeeze kit. Typical conjugate concentrations were 100−300 nM. The final buffer of the AuNS-conjugates is presumed to be 1×TAE, with some residual BSPP and NaCl. There may also be some residue from the Freeze 'N Squeeze product and from the agarose gel.

DOI: 10.1021/acsnano.6b07291
ACS Nano 2017, 11, 831−842

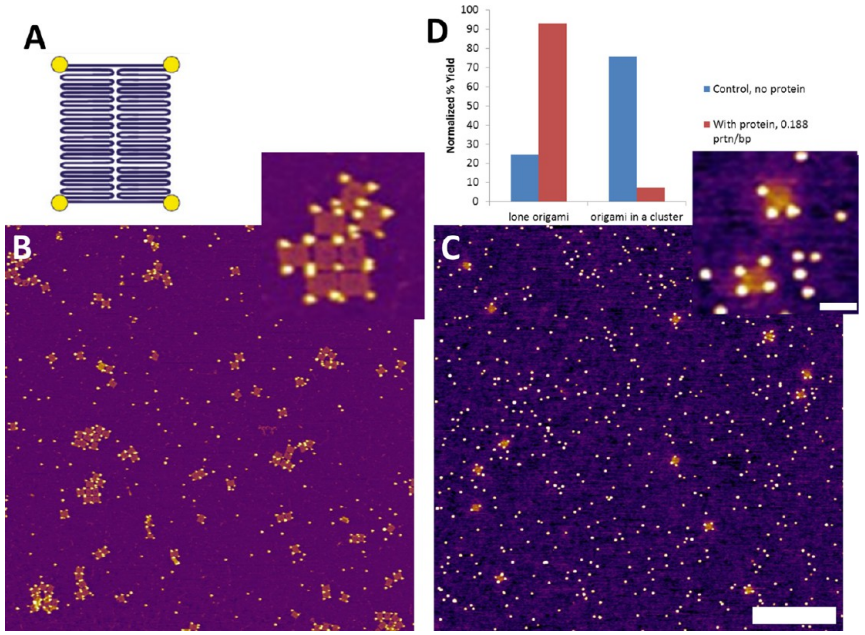

Figure 11. (A) Schematic of desired architecture of tall rectangle DNA origamis hybridized with one AuNS at each corner. Dry AFM images of (B) the control sample without protein protection and (C) the sample protected with 0.188 C_8–B^{Sso7d} protein/bp before hybridization. (D) Analysis of origami–AuNS complexes in clusters (undesired) *vs* lone structures (desired) without protein (blue) and with protein (red). Scale bar is 1 μm. Inset scale bar is 100 nm.

Preparation of DNA-Coated AuNRs. Following the published recipe,[68] thiolated DNA strands were reduced using TCEP-coated polystyrene beads and 0.75×TE buffer. AuNRs were then washed of excess CTAB by melting the CTAB and subsequently centrifuging the AuNR/CTAB solution at 4700 *g* for 10 min, so that the AuNRs form a pellet in the bottom of the tube. The supernatant was removed and replaced with 0.01% SDS, and the centrifuge purification was repeated for a total of 3 times, wherein the last resuspension comprises one-tenth of the original volume so as to concentrate the AuNR solution. Reduced, thiolated DNA was immediately added to the solution and shaken for a few hours. The solution was then brought to 1×TBE and shaken overnight. The solution was then slowly brought to 0.5 M NaCl over 24–48 h and incubated overnight. Excess thiolated DNA was removed by centrifugation, removing the supernatant and replacing it with 1×TBE/0.01% SDS for a total of five rinses.

Preparation of Protein–DNA Origami or Protein–AuNP Complexes. Protein–DNA origami complexes were prepared by mixing aliquots of DNA origami stock solution (in 1×TAEMg) and protein stock solution (0.25 to 2 g/L in 10 mM acetate buffer, pH 4.85). Protein–AuNP complexes were prepared by mixing aliquots of AuNP stock solutions (1×TAE or 1×TBE for AuNSs or AuNRs, respectively) and protein stock solution. Mixtures were vortexed for 10 s. Volumes of the mixed portions of stock DNA or AuNP and protein solutions were varied according to their initial concentration and the desired final protein/DNA-bp (protein/bp) ratio.

Electrophoretic Mobility Shift Assay. Aliquots of 5 nM origami (40 ng/μL) in 1×TAEMg were mixed with different volumes of a C_8–B^{Sso7d} solution (0.25 to 2 g/L) in 10 mM acetate buffer, pH 4.85. Mixtures were vortexed for 10 s and then incubated for 60 min at room temperature. The solutions were mixed with 50% glycerol to a final concentration of 10% glycerol and subjected to electrophoresis in an agarose gel (1% agarose, 1×TAEMg) for 30 min at 90 V using 1×TAEMg running buffer. Bands were visualized using EtBr.

Atomic Force Microscopy. Dry imaging: 1 μL of protein–DNA origami (–AuNP) complex (1–5 nM origami) solution was mixed with 9 μL of filtered Milli-Q water and immediately added to a freshly cleaved mica surface (1 cm diameter) and left for 3 min. Then it was rinsed with 50 μL of filtered Milli-Q water for 2 s to remove salts and nonabsorbed particles, followed by slow drying under a N_2 stream. Samples were analyzed using an Asylum Cypher equipped with a silicon nitride DNP-S probe (Bruker) with a spring constant of 0.35 N/m in AC Molecule tapping mode. Images were recorded at 1.95 Hz and 512 samples per line. Height profile measurements were performed with the Igor software. For control samples without protein, wet imaging was performed, as specified below.

Wet imaging (for solubilization and release-time experiments): 5 μL of solution containing equal molar amounts of two DNA origami shapes (~0.5 nM of each origami type) in 1×TAEMg was pipetted onto a freshly cleaved mica surface and left for 3 min. Then 50 μL of 1×TAEMg was added, and samples were analyzed using an Asylum Cypher equipped with a silicon BioLever Mini probe in AC Molecule fluid imaging tapping mode. After an initial image was recorded, C_8–B^{Sso7d} solution (0.25 to 2 g/L) in 10 mM acetate buffer, pH 4.85, was added to bring the final protein/bp concentration to a given value. The solution was pipetted up and down for mixing, and AFM was performed every few minutes for up to 2 h. Images were recorded at 1.95 Hz and 512 samples per line.

DNase Protection Test. DNA origami 7.2 kbp (concentration of 20–40 ng/μL) was complexed with C_8–B^{Sso7d} in 10 mM acetate buffer (0.188 protein/bp final) for 1 h at room temperature. Then the enzyme DNase I dissolved in reaction DNase I buffer (100 mM Tris-HCl, pH 7.5, 25 mM $MgCl_2$, 1 mM $CaCl_2$) was added to bring the final concentration to 0.4 U DNase I/μg DNA. Aliquots of 3.5 μL were taken at different times and mixed with 3.5 μL of 50 mM EDTA. After an addition of loading buffer (final concentration of 10% glycerol), the sample was electrophoresed in agarose gel (1%, 1×TAEMg) at 100 V for 20 min. DNA bands were visualized using EtBr.

UV–vis Spectroscopy. Solutions of 100 nM DNA-coated AuNP were mixed either with C_8–B^{Sso7d} in 10 mM acetate buffer (to bring the final solution to 0.188 protein/bp) or an equal volume of 10 mM acetate buffer without any protein (for the control sample). Aliquots of 1.5 μL were pipetted onto the sample stage of a Nanodrop UV–vis spectroscope, and data were collected from 260 to 780 nm wavelengths. The samples were then brought to 25 mM Mg^{2+} using a 1 M Mg acetate stock solution, and 1.5 μL aliquots were taken to collect UV–vis spectroscopy data at various times. The same procedure was performed for 80 nM DNA-coated AuNR solutions.

DOI: 10.1021/acsnano.6b07291
ACS Nano 2017, 11, 831–842

ASSOCIATED CONTENT

Supporting Information

The Supporting Information is available free of charge on the ACS Publications website at DOI: 10.1021/acsnano.6b07291.

The design and DNA sequences associated with the tetrahedral DNA origami, additional AFM images and electrophoretic assay figures relating to protein compatibilization, and calculations of number of proteins per base pair of DNA (PDF)

AUTHOR INFORMATION

Corresponding Author

*E-mail: naestric@ncsu.edu.

ORCID

Nicole A. Estrich: 0000-0001-7042-5440

Armando Hernandez-Garcia: 0000-0001-5505-3423

Thomas H. LaBean: 0000-0002-6739-2059

Notes

The authors declare no competing financial interest.

ACKNOWLEDGMENTS

The authors acknowledge financial support from the National Science Foundation through NSF-ECCS-EPMD-1231888 to T.H.L. R.d.V. and A.H.G. acknowledge financial support of the Dutch Polymer Institute, project 698. A.H.G. acknowledges financial support of CONACYT, Mexico (scholarship for graduate studies).

REFERENCES

(1) Seeman, N. C. DNA in a Material World. *Nature* **2003**, *421*, 427−431.

(2) Li, H.; Carter, J. D.; LaBean, T. H. Nanofabrication by DNA Self-Assembly. *Mater. Today* **2009**, *12*, 24−32.

(3) Rothemund, P. W. K. Folding DNA to Create Nanoscale Shapes and Patterns. *Nature* **2006**, *440*, 297−302.

(4) Saaem, I.; Labean, T. H. Overview of DNA Origami for Molecular Self-Assembly. *WIREs Nanomed. Nanobiotechnol.* **2013**, *5*, 150−162.

(5) Torring, T.; Voigt, N. V.; Nangreave, J.; Yan, H.; Gothelf, K. V. DNA Origami: A Quantum Leap for Self-Assembly of Complex Structures. *Chem. Soc. Rev.* **2011**, *40*, 5636−5646.

(6) Martin, T. G.; Dietz, H. Magnesium-Free Self-Assembly of Multi-Layer DNA Objects. *Nat. Commun.* **2012**, *3*, 1103.

(7) Naora, H.; Izawa, M.; Allfrey, V. G.; Mirsky, A. E. Some Observations on Differences in Composition Between the Nucleus and Cytoplasm of the Frog Oocyte. *Proc. Natl. Acad. Sci. U. S. A.* **1962**, *48*, 853−859.

(8) Billett, M. A.; Barry, J. M. Role of Histones in Chromatin Condensation. *Eur. J. Biochem.* **1974**, *49*, 477−484.

(9) Hooper, G.; Dick, D. A. Nonuniform Distribution of Sodium in the Rat Hepatocyte. *J. Gen. Physiol.* **1976**, *67*, 469−474.

(10) Moore, R. D.; Morrill, G. A. A Possible Mechanism for Concentrating Sodium and Potassium in the Cell Nucleus. *Biophys. J.* **1976**, *16*, 527−533.

(11) Bakshi, S. R.; Batista, R. G.; Agarwal, A. Quantification of Carbon Nanotube Distribution and Property Correlation in Nanocomposites. *Composites, Part A* **2009**, *40*, 1311−1318.

(12) Niyogi, S.; Hamon, M. A.; Hu, H.; Zhao, B.; Bhowmik, P.; Sen, R.; Itkis, M. E.; Haddon, R. C. Chemistry of Single-Walled Carbon Nanotubes. *Acc. Chem. Res.* **2002**, *35*, 1105−1113.

(13) Rabotyagova, O. S.; Cebe, P.; Kaplan, D. L. Protein-Based Block Copolymers. *Biomacromolecules* **2011**, *12*, 269−289.

(14) Meyer, D. E.; Chilkoti, A. Genetically Encoded Synthesis of Protein-Based Polymers with Precisely Specified Molecular Weight and Sequence by Recursive Directional Ligation: Examples from the Elastin-like Polypeptide System. *Biomacromolecules* **2002**, *3*, 357−367.

(15) Urry, D. W. Physical Chemistry of Biological Free Energy Transduction As Demonstrated by Elastic Protein-Based Polymers †. *J. Phys. Chem. B* **1997**, *101*, 11007−11028.

(16) Zhang, X.; Urry, D. W.; Daniell, H. Expression of an Environmentally Friendly Synthetic Protein-Based Polymer Gene in Transgenic Tobacco Plants. *Plant Cell Rep.* **1996**, *16*, 174−179.

(17) Krejchi, M. T.; Atkins, E. D.; Waddon, A. J.; Fournier, M. J.; Mason, T. L.; Tirrell, D. A. Chemical Sequence Control of Beta-Sheet Assembly in Macromolecular Crystals of Periodic Polypeptides. *Science* **1994**, *265*, 1427−1432.

(18) Link, A. J.; Mock, M. L.; Tirrell, D. A. Non-Canonical Amino Acids in Protein Engineering. *Curr. Opin. Biotechnol.* **2003**, *14*, 603−609.

(19) Yoshikawa, E.; Fournier, M. J.; Mason, T. L.; Tirrell, D. A. Genetically Engineered Fluoropolymers. Synthesis of Repetitive Polypeptides Containing p-Fluorophenylalanine Residues. *Macromolecules* **1994**, *27*, 5471−5475.

(20) Kiick, K.; van Hest, J. C.; Tirrell, D. Expanding the Scope of Protein Biosynthesis by Altering the Methionyl-tRNA Synthetase Activity of a Bacterial Expression Host. *Angew. Chem., Int. Ed.* **2000**, *39*, 2148−2152.

(21) Kwon, I.; Kirshenbaum, K.; Tirrell, D. A. Breaking the Degeneracy of the Genetic Code. *J. Am. Chem. Soc.* **2003**, *125*, 7512−7513.

(22) Wang, P.; Tang, Y.; Tirrell, D. A. Incorporation of Trifluoroisoleucine into Proteins *in vivo*. *J. Am. Chem. Soc.* **2003**, *125*, 6900−6906.

(23) Connor, R. E.; Tirrell, D. A. Non-Canonical Amino Acids in Protein Polymer Design. *Polym. Rev.* **2007**, *47*, 9−28.

(24) Hernandez-Garcia, A.; Werten, M. W. T.; Stuart, M. C.; de Wolf, F. A.; de Vries, R. Coating of Single DNA Molecules by Genetically Engineered Protein Diblock Copolymers. *Small* **2012**, *8*, 3491−3501.

(25) Hernandez-Garcia, A.; Kraft, D. J.; Janssen, A. F. J.; Bomans, P. H. H.; Sommerdijk, N. A. J. M.; Thies-Weesie, D. M. E.; Favretto, M. E.; Brock, R.; de Wolf, F. A.; Werten, M. W. T.; van der Schoot, P.; Cohen Stuart, M.; de Vries, R. Design and Self-Assembly of Simple Coat Proteins for Artificial Viruses. *Nat. Nanotechnol.* **2014**, *9*, 698−702.

(26) Hernandez-Garcia, A.; Estrich, N. A.; Werten, M. W. T.; Van Der Maarel, J. R. C.; LaBean, T. H.; de Wolf, F. A.; Cohen Stuart, M. A.; de Vries, R. J. Precise Coating of a Wide Range of DNA Templates by a Protein Polymer with a DNA Binding Domain. *ACS Nano* **2016**, Article ASAP. 10.1021/acsnano.6b05938

(27) Werten, M. W.; Wisselink, W. H.; Jansen-van den Bosch, T. J.; de Bruin, E. C.; de Wolf, F. A. Secreted Production of a Custom-Designed, Highly Hydrophilic Gelatin in Pichia pastoris. *Protein Eng., Des. Sel.* **2001**, *14*, 447−454.

(28) Zhang, C.; Hernandez-Garcia, A.; Jiang, K.; Gong, Z.; Guttula, D.; Ng, S. Y.; Malar, P. P.; van Kan, J. A.; Dai, L.; Doyle, P. S.; de Vries, R.; van der Maarel, J. R. Amplified Stretch of Bottlebrush-Coated DNA in Nanofluidic Channels. *Nucleic Acids Res.* **2013**, *41*, e189.

(29) Gera, N.; Hill, A. B.; White, D. P.; Carbonell, R. G.; Rao, B. M. Design of pH Sensitive Binding Proteins from the Hyperthermophilic Sso7d Scaffold. *PLoS One* **2012**, *7*, e48928.

(30) Baumann, H.; Knapp, S.; Karshikoff, A.; Ladenstein, R.; Härd, T. DNA-Binding Surface of the Sso7d Protein from Sulfolobus solfataricus. *J. Mol. Biol.* **1995**, *247*, 840−846.

(31) Gao, Y. G.; Su, S. Y.; Robinson, H.; Padmanabhan, S.; Lim, L.; McCrary, B. S.; Edmondson, S. P.; Shriver, J. W.; Wang, A. H. The Crystal Structure of the Hyperthermophile Chromosomal Protein Sso7d Bound to DNA. *Nat. Struct. Biol.* **1998**, *5*, 782−786.

(32) Agback, P.; Baumann, H.; Knapp, S.; Ladenstein, R.; Härd, T. Architecture of Nonspecific Protein-DNA Interactions in the Sso7d-DNA Complex. *Nat. Struct. Biol.* **1998**, *5*, 579−584.

(33) Murphy, F. V.; Churchill, M. E. Nonsequence-Specific DNA Recognition: a Structural Perspective. *Structure* **2000**, *8*, R83−R89.

(34) Martens, A. A.; Portale, G.; Werten, M. W. T.; de Vries, R. J.; Eggink, G.; Cohen Stuart, M. A.; de Wolf, F. A. Triblock Protein Copolymers Forming Supramolecular Nanotapes and pH-Responsive Gels. *Macromolecules* **2009**, *42*, 1002−1009.
(35) Zhang, F.; Jiang, S.; Wu, S.; Li, Y.; Mao, C.; Liu, Y.; Yan, H. Complex Wireframe DNA Origami Nanostructures with Multi-Arm Junction Vertices. *Nat. Nanotechnol.* **2015**, *10*, 779−784.
(36) Iinuma, R.; Ke, Y.; Jungmann, R.; Schlichthaerle, T.; Woehrstein, J. B.; Yin, P. Polyhedra Self-Assembled from DNA Tripods and Characterized with 3D DNA-PAINT. *Science* **2014**, *344*, 65−69.
(37) Douglas, S. M.; Dietz, H.; Liedl, T.; Högberg; Graf, F.; Shih, W. M. Self-Assembly of DNA into Nanoscale Three-Dimensional Shapes. *Nature* **2009**, *459*, 414−418.
(38) Ko, S. H.; Su, M.; Zhang, C.; Ribbe, A. E.; Jiang, W.; Mao, C. Synergistic Self-Assembly of RNA and DNA Molecules. *Nat. Chem.* **2010**, *2*, 1050−1055.
(39) Tian, Y.; Wang, T.; Liu, W.; Xin, H. L.; Li, H.; Ke, Y.; Shih, W. M.; Gang, O. Prescribed Nanoparticle Cluster Architectures and Low-Dimensional Arrays Built Using Octahedral DNA Origami Frames. *Nat. Nanotechnol.* **2015**, *10*, 637−644.
(40) Shih, W. M.; Quispe, J. D.; Joyce, G. F. A 1.7-kilobase Single-Stranded DNA that Folds into a Nanoscale Octahedron. *Nature* **2004**, *427*, 618−621.
(41) Han, D.; Pal, S.; Nangreave, J.; Deng, Z.; Liu, Y.; Yan, H. DNA Origami with Complex Curvatures in Three-Dimensional Space. *Science* **2011**, *332*, 342−346.
(42) Dietz, H.; Douglas, S. M.; Shih, W. M. Folding DNA into Twisted and Curved Nanoscale Shapes. *Science* **2009**, *325*, 725−730.
(43) Marchi, A. N.; Saaem, I.; Vogen, B. N.; Brown, S.; LaBean, T. H. Toward Larger DNA Origami. *Nano Lett.* **2014**, *14*, 5740−5747.
(44) Marchi, A. N.; Saaem, I.; Tian, J.; LaBean, T. H. One-Pot Assembly of a Hetero-Dimeric DNA Origami from Chip-Derived Staples and Double-Stranded Scaffold. *ACS Nano* **2013**, *7*, 903−910.
(45) Zhao, Z.; Liu, Y.; Yan, H. Organizing DNA Origami Tiles into Larger Structures Using Preformed Scaffold Frames. *Nano Lett.* **2011**, *11*, 2997−3002.
(46) Yang, Y.; Zhao, Z.; Zhang, F.; Nangreave, J.; Liu, Y.; Yan, H. Self-Assembly of DNA Rings from Scaffold-Free DNA Tiles. *Nano Lett.* **2013**, *13*, 1862−1866.
(47) Lin, C.; Liu, Y.; Rinker, S.; Yan, H. DNA Tile Based Self-Assembly: Building Complex Nanoarchitectures. *ChemPhysChem* **2006**, *7*, 1641−1647.
(48) Kim, K. R.; Lee, Y. D.; Lee, T.; Kim, B. S.; Ahn, D. R. Sentinel Lymph Node Imaging by a Fluorescently Labeled DNA Tetrahedron. *Biomaterials* **2013**, *34*, 5226−5235.
(49) Li, Z.; Wei, B.; Nangreave, J.; Lin, C.; Liu, Y.; Mi, Y.; Yan, H. A Replicable Tetrahedral Nanostructure Self-Assembled from a Single DNA Strand. *J. Am. Chem. Soc.* **2009**, *131*, 13093−13098.
(50) Goodman, R. P.; Heilemann, M.; Doose, S.; Erben, C. M.; Kapanidis, A. N.; Turberfield, A. J. Reconfigurable, Braced, Three-Dimensional DNA Nanostructures. *Nat. Nanotechnol.* **2008**, *3*, 93−96.
(51) Bu, N. N.; Gao, A.; He, X. W.; Yin, X. B. Electrochemiluminescent Biosensor of ATP using Tetrahedron Structured DNA and a Functional Oligonucleotide for Ru(phen)32+ Intercalation and Target Identification. *Biosens. Bioelectron.* **2013**, *43*, 200−204.
(52) Mastroianni, A. J.; Claridge, S.; Alivisatos, A. P. Pyramidal and Chiral Grouping of Gold Nanocrystals Assembled Usign DNA Scaffolds. *J. Am. Chem. Soc.* **2009**, *131*, 8455−8459.
(53) Özhalici-Ünal, H.; Armitage, B. A. Fluorescent DNA Nanotags Based on a Self-Assembled DNA Tetrahedron. *ACS Nano* **2009**, *3*, 425−433.
(54) Liu, Z.; Li, Y.; Tian, C.; Mao, C. A Smart DNA Tetrahedron that Isothermally Assembles or Dissociates in Response to the Solution pH Value Changes. *Biomacromolecules* **2013**, *14*, 1711−1714.
(55) Kato, T.; Goodman, R. P.; Erben, C. M.; Turberfield, A. J.; Namba, K. High-Resolution Structural Analysis DNA Nanostructure by CryoEM. *Nano Lett.* **2009**, *9*, 2747−2750.
(56) Yan, W.; Xu, L.; Xu, C.; Ma, W.; Kuang, H.; Wang, L.; Kotov, N. A. Self-Assembly of Chiral Nanoparticle Pyramids with Strong R/S Optical Activity. *J. Am. Chem. Soc.* **2012**, *134*, 15114−15121.
(57) Wilks, T. R.; Bath, J.; de Vries, J. W.; Raymond, J. E.; Herrmann, A.; Turberfield, A. J.; O'Reilly, R. K. 'Giant Surfactants' Created by the Fast and Efficient Functionalization of a DNA Tetrahedron with a Temperature-Responsive Polymer. *ACS Nano* **2013**, *7*, 8561−8572.
(58) He, Y.; Ye, T.; Su, M.; Zhang, C.; Ribbe, A. E.; Jiang, W.; Mao, C. Hierarchical Self-Assembly of DNA into Symmetric Supramolecular Polyhedra. *Nature* **2008**, *452*, 198−201.
(59) Wong, N. Y.; Zhang, C.; Tan, L. H.; Lu, Y. Site-Specific Attachment of Proteins onto a 3D DNA Tetrahedron Through Backbone-Modified Phosphorothioate DNA. *Small* **2011**, *7*, 1427−1430.
(60) Schlapak, R.; Danzberger, J.; Armitage, D.; Morgan, D.; Ebner, A.; Hinterdorfer, P.; Pollheimer, P.; Gruber, H. J.; Schäffler, F.; Howorka, S. Nanoscale DNA Tetrahedra Improve Biomolecular Recognition on Patterned Surfaces. *Small* **2012**, *8*, 89−97.
(61) Douglas, S. M.; Marblestone, A. H.; Teerapittayanon, S.; Vazquez, A.; Church, G. M.; Shih, W. M. Rapid Prototyping of 3D DNA-Origami Shapes with caDNAno. *Nucleic Acids Res.* **2009**, *37*, 5001−5006.
(62) Castro, C. E.; Kilchherr, F.; Kim, D.-N.; Shiao, E. L.; Wauer, T.; Wortmann, P.; Bathe, M. A Primer to Scaffolded DNA Origami. *Nat. Methods* **2011**, *8*, 221−229.
(63) Kim, D.-N.; Kilchherr, F.; Dietz, H.; Bathe, M. Quantitative Prediction of 3D Solution Shape and Flexibility of Nucleic Acid Nanostructures. *Nucleic Acids Res.* **2012**, *40*, 2862−2868.
(64) Pan, K.; Kim, D.-N.; Zhang, F.; Adendorff, M. R.; Yan, H.; Bathe, M. Lattice-Free Prediction of Three-Dimensional Structure of Programmed DNA Assemblies. *Nat. Commun.* **2014**, *5*, 5578.
(65) Piétrement, O.; Pastré, D.; Fusil, S.; Jeusset, J.; David, M.-O.; Landousy, F.; Hamon, L.; Zozime, A.; Le Cam, E. Reversible Binding of DNA on NiCl 2 -Treated Mica by Varying the Ionic Strength. *Langmuir* **2003**, *19*, 2536−2539.
(66) Woo, S.; Rothemund, P. W. K. Self-Assembly of Two-Dimensional DNA Origami Lattices Using Cation-Controlled Surface Diffusion. *Nat. Commun.* **2014**, *5*, 4889.
(67) Pilo-Pais, M.; Goldberg, S.; Samano, E.; Labean, T. H.; Finkelstein, G. Connecting the Nanodots: Programmable Nanofabrication of Fused Metal Shapes on DNA Templates. *Nano Lett.* **2011**, *11*, 3489−3492.
(68) Pal, S.; Deng, Z.; Wang, H.; Zou, S.; Liu, Y.; Yan, H. DNA Directed Self-Assembly of Anisotropic Plasmonic Nanostructures. *J. Am. Chem. Soc.* **2011**, *133*, 17606−17609.
(69) Brown, S.; Jespersen, T. S.; Nygård, J. A Genetic Analysis of Carbon-Nanotube-Binding Proteins. *Small* **2008**, *4*, 416−420.
(70) Kozek, K. A.; Kozek, K. M.; Wu, W.-C.; Mishra, S. R.; Tracy, J. B. Large-Scale Synthesis of Gold Nanorods through Continuous Secondary Growth. *Chem. Mater.* **2013**, *25*, 4537−4544.
(71) Kundukad, B.; van der Maarel, J. R. C. Control of the Flow Properties of DNA by Topoisomerase II and its Targeting Inhibitor. *Biophys. J.* **2010**, *99*, 1906−1915.
(72) Loweth, C. J.; Caldwell, W. B.; Peng, X.; Alivisatos, A. P.; Schultz, P. G. DNA-Based Assembly of Gold Nanocrystals. *Angew. Chem., Int. Ed.* **1999**, *38*, 1808−1812.
(73) Zanchet, D.; Micheel, C. M.; Parak, W. J.; Gerion, D.; Alivisatos, A. P. Electrophoretic Isolation of Discrete Au Nanocrystal/DNA Conjugates. *Nano Lett.* **2001**, *1*, 32−35.

DOI: 10.1021/acsnano.6b07291
ACS Nano 2017, 11, 831−842